Enhancing the safety and stability of lithium metal batteries through the use of composite ionogels

Enhancing the safety and stability of lithium metal batteries through the use of composite ionogels.

Matteo Gandolfo,[1] Daniele Versaci, [1] Carlotta Francia,[1] Silvia Bodoardo,[1] Julia Amici,[1*]

[1] Department of Applied Science and Technology, Politecnico di Torino, Corso Duca degli Abruzzi 24, 10129 – Torino, Italy

Corresponding author: julia.amici@polito.it

Abstract:

Solid-state polymer electrolytes are a promising platform for safer lithium-metal batteries, but low ionic conductivity and high interfacial resistance with electrodes limit the room temperature applications. Herein, an ionogel (IG) composed of a crosslinked polymer matrix and an ionic liquid (PYR14TFSI), prepared through a one-pot thermal polymerization has been investigated. Alumina nanoparticles (Al_2O_3 NPs) were added into this IG to further increase ionic conductivity and cycling performances, by coordinating anionic species at the surface of the inorganic filler, promoting the Li^+ motion. The alumina composite IG shows an ionic conductivity of $2.05 \cdot 10^{-4}$ S cm^{-1} at 20 °C such as a wide electrochemical stability window (ESW) of 5.12 V vs. Li^+/Li. The $LiFePO_4/Li$ batteries assembled with different IGs present good cycling performance at room temperature, interesting capacity retention after 500 cycles at 0.2 C and more importantly, improved capacity even at 1 C, compared to the ionic liquid alone soaked on a glass fiber separator. This work provides a simple approach to prepare safer composite IG with remarkable electrochemical performances at room temperature for lithium metal batteries.

Keywords: ionogel; metallic lithium; safety; cross-linked polymer; inorganic additive

Graphical abstract:

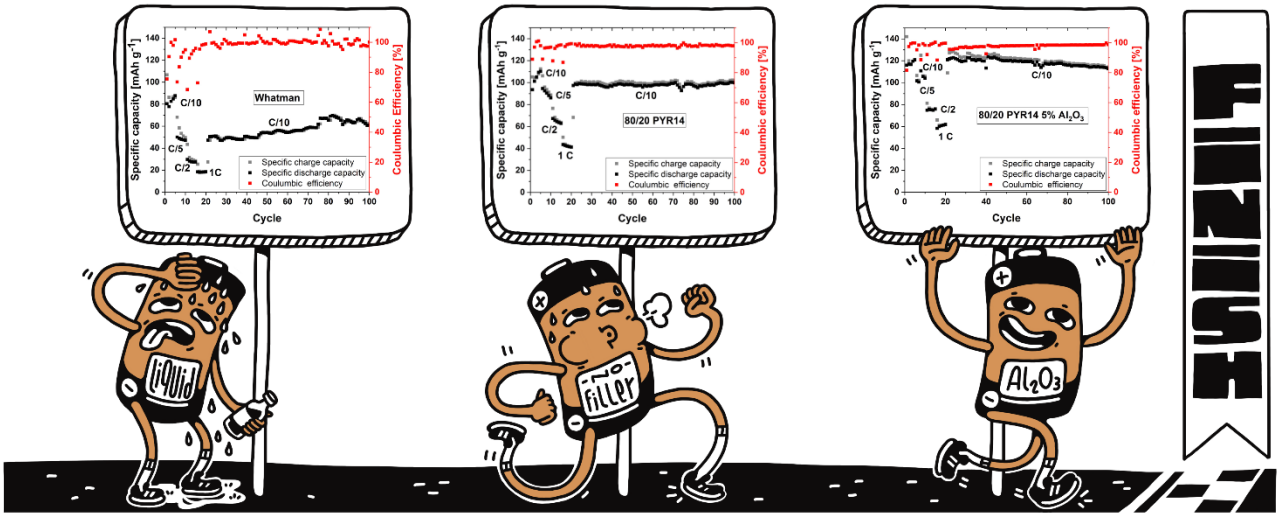

Introduction:

lithium-ion batteries (LIBs) are a well-exploited technology since their first commercialization in the 90s and have proven to be an efficient energy storage system. LIB applications jumped recently with the need to reduce greenhouse gas emissions and store energy produced from intermittent renewable power sources, like wind and sun, but earlier, in the first years of the new millennium, LIBs powered the revolution in portable electronics [1]. Despite being a young technology, LIBs are reaching their theoretical energy density (~ 350 Wh kg^{-1}) and struggle to meet the market requests in many sectors, like the automotive one. In this direction, lithium metal anode is considered the "holy Grail" for potentially doubling the energy density as compared with the state of art LIBs, due to the promising high theoretical specific capacity (3860 mAh g^{-1}) and the lowest redox potential (- 3.04 V *vs.* SHE) [2]. However, uncontrollable dendrite growth and high reactivity of lithium metal anode lead to scarce cycling efficiency, cause important safety issues and draw the liquid electrolyte producing a thick SEI layer [3].

Solid-state electrolytes (SSEs) have been investigated as a replacement for liquid ones to increase the energy density and cell safety of LMBs. In this frame, SSEs made of a polymer matrix with a dissolved lithium salt are promising electrolytes due to their good interfacial contact with electrodes

and high flexibility. These solid polymer electrolytes (SPEs) have been largely investigated starting from the first studies in 1973 by Wright and co-workers on the dissolution of lithium salts in polyethylene oxide (PEO) [4] and in 1978 when Armand developed the Li^+ conduction mechanism in PEO-based polymer electrolyte [5]. The scarce ionic conduction of the polymer matrix encouraged Feuillade in 1975 to add a plasticizer developing the first quasi-solid state gel polymer electrolyte (GPE) made of poly(vinylidene fluoride-co-hexafluoropropylene (PVDF-HFP) with propylene carbonate (PC) [6].

In the following years, PEO had a dominant role in the development of polymer electrolytes, but different polymer matrices were also investigated such as poly(vinylidene fluoride) (PVdF) [7,8], polyacrylonitrile (PAN) [9,10], polymethyl methacrylate (PMMA) [11,12], poly(1,3-dioxolane) (PDOL) [13,14] and poly(propylene carbonate) (PPC) [15,16]. The addition of inorganic filler to polymer electrolytes and the effect on the electrochemical properties were also studied in developing composite polymer electrolytes (CPEs). In 1988, Skaarup et al. incorporated the lithium-conductor filler Li_3N into a PEO matrix, obtaining an improvement of three orders of magnitude in the ionic conductivity compared to the pure polymer [17] and Wieczorek et al. found that the addition of Al_2O_3 particles could improve the ionic conductivity of a PEO-based polymer electrolyte [18]. So far, different hybrid electrolytes have been studied with the incorporation of passive filler, non-conductive for Li^+ ions, like Al_2O_3 [19,20] SiO_2 [21], TiO_2 [22], ZrO_2 [23], and active filler, Li^+ ion-conductor, such as $Li_7La_3Zr_2O_{12}$ (LLZO) [24], $Li_{6.4}La_3Zr_{1.4}Ta_{0.6}O_{12}$ (LLZTO) [25], $Li_{1.5}Al_{0.5}Ge_{1.5}(PO_4)_3$ (LAGP) [26], $Li_{1.3}Al_{0.3}Ti_{1.7}P(O_4)_3$ (LATP) [27]. Inorganic fillers are responsible for the enhancement of different polymer electrolyte properties. The crystallinity of the polymer matrix can be largely decreased and the dissociation of lithium salts can be favoured by the addition of ceramic particles, with a beneficial effect on the ionic conductivity [28]. Additionally, some active fillers can form an effective pathway for Li^+ motion by tuning the amount of ceramic particles [29]. Furthermore, inorganic fillers affect the mechanical properties by creating a rigid skeleton in the polymer matrix

increasing the stiffness with a positive effect against lithium dendrites growth [30]. The effect on the polymer electrolyte is strictly related to the size, morphology and surface group of such inorganic fillers [31],[32],[33].

Plasticizers have been largely used to improve the ionic conductivity and the scarce interfaces with electrodes of SPE. Combining the advantages of liquid and solid electrolytes, GPE is a widely studied platform for fast Li^+ conduction. Organic solvents commonly used as plasticizers include carbonates like ethylene carbonate (EC), propylene carbonate (PC), diethyl carbonate (DEC), dimethyl carbonate (DMC), but also dimethyl formamide (DMF), dimethyl sulphoxide (DMSO) and tetrahydrofuran (THF). Unfortunately, most of the organic solvents are extremely volatile, flammable, toxic and environmentally hazardous, which seriously limits the application in LMBs [34]. Recently, huge efforts were devoted to replace conventional organic solvents with safer ionic liquids (ILs). As low melting point organic salts, ILs have ion conducting capability, non-flammability, non-volatility, large electrochemical stability window (up to 6 V *vs.* Li^+/Li) and good thermal stability [35]. Aprotic ILs, used in the battery field, are composed of a large organic cation such as pyridinium, imidazolium and phosphonium coupled with smaller anions (e.g. bromine (Br^-), chloride (Cl^-), hexafluorophosphate (PF_6^-)) and organic anions (e.g. bis(trifluoromethyl sulfonyl)imide ($TFSI^-$), bis(fluoro sulfonyl)imide (FSI^-)) [36]. Such ILs have been added into polymer matrices as plasticizers forming ionogels (IGs), with enhanced safety compared to conventional GPE. Although ILs possess interesting properties, the addition of inorganic particles to IGs is still needed to further increase the electrochemical performances and mechanical strength. The thickness is also an important parameter to be reduced by correctly tuning the polymer matrix and the inorganic skeleton [37,38].

Zheng et al. developed an IG blending methyl methacrylate (MMA), N-butyl-N-methyl-piperidinium (PYR14TFSI) and lithium salts with SiO_2 and $Li_{0.33}La_{0.56}TiO_3$ (LLTO) additives [39]. The prepared MMA-PYR14TFSI-3 wt% LLTO delivered an ion conductivity of 4.51×10^{-3} S cm^{-1} at 60 °C and an electrochemical stability window up to 5.0 V (*vs.* Li^+/Li). With the synergic effect of both

inorganic fillers, the IG achieved an initial discharge capacity of 150 mAh g^{-1} at 0.5 C with good capacity retention under 60 °C in a half-cell configuration with lithium metal anode and LFP cathode. Liao et al. prepared a polyethylene-supported SiO_2/poly(methyl methacrylate–acrylonitrile–vinyl acetate) (P(MMA–AN–VAc)) and Al_2O_3/P(MMA–AN–VAc) both of them added with PYR14TFSI and vinylene carbonate (VC) [40]. The inorganic nanoparticles improved the ionic conductivity by forming Lewis acid–base interactions and providing more lithium ion conducting pathways. The addition of ceramic fillers increased the electrochemical stability window up to 5.25 V and 5.3 V (*vs.* Li/Li^+) for Al_2O_3 and SiO_2 electrolyte compared to 5.0 V (*vs.* Li/Li^+) of no filler electrolyte, and delivered the same initial discharge capacity (~140 mAh g^{-1}) at 0.1 C sandwiched between Lithium metal anode and LFP cathode with a lower capacity fade for SiO_2 electrolyte.

In this work, we developed a solvent-less composite IG composed of an acrylate-based polymer matrix and alumina nanoparticles. The self-standing and flexible membranes were obtained in a one-pot preparation method through thermally induced radical polymerization. The high content of IL and the addition of Al_2O_3 NPs boosted the electrochemical performances, obtaining remarkable ionic conductivity ($2.5 \cdot 10^{-4}$ S cm^{-1} at 20 °C) and wide electrochemical stability window (5.1 V *vs.* lithium metal) and good cycling performances at room temperature after 500 cycles. The results were compared to the no filler IG highlighting a reduced polarization, a better interfacial forming capability and an increased transport number for Al_2O_3 NPs IG, resulting in far better rate performance.

Experimental:

The IGs synthesis was performed in an Ar-filled glovebox (Mbraun labstar with O_2 and H_2O below < 0.5 ppm) to avoid oxygen inhibition of free-radical polymerization. Butyl methacrylate (BMA) was purchased from Acros Organics, poly(ethylene glycol) diacrylate (PEGDA) (average M_n 575), aluminium oxide nanoparticles (Al_2O_3 NP_s) and lithium bis(trifluoromethanesulfonyl)imide (LITFSI) were supplied by Sigma-Aldrich and 1-Butyl-1-methylpyrrolidinium bis(trifluoromethylsulfonyl)imide (PYR14 TFSI) was provided by Solvionic. The IG labelled as

80/20 PYR14 was prepared by mixing the monomer mixture, PYR14 TFSI and LITFSI respectively in a 1:3:1 weight ratio, in which the monomer mixture was composed of BMA and PEGDA respectively in a 4:1 weight ratio. In another formulation, the addition of 5% wt of Al_2O_3 NP_s compared to the polymer matrix was also investigated and this formulation was named 80/20 PYR14 5% Al_2O_3. The thermo-initiator benzoyl peroxide (BPO, 75% Acros Organics) was added in a proportion of 1% wt in both formulations. The mixture was heated to 65 °C for 20 min to start the polymerization, then cast on a glass slide and kept at 55 °C for 20 h.

The $LiFePO_4$ (LFP) cathode was used as the testing electrode, produced by mixing LFP (Aleess), Carbon black C-NERGY C65 (Timcal Imeyrs) and polyvinylidene fluoride (PVdF, HSV900, Arkema) in a 7:2:1 weight ratio with N-methyl pyrrolidone (NMP) as solvent. The slurry obtained was homogenized in a mixer mill (Retsch® MM40), deposited on Al foil with a doctor blade film applicator and dried at 50 °C for 90 min. Electrodes were cut into 15 mm diameter discs, dried under vacuum at 120 °C for 4 h and stored in an Ar-filled glovebox, the final mass loading was 2 mg cm^{-2}.

The surface and cross-section of IGs were acquired with a Zeiss SUPRA TM 40 with Gemini column and Schottky field emission tip (tungsten at 1800 K) FE-SEM.

The thermal stability of IGs was evaluated by thermogravimetric analysis (TGA) in the temperature range 25-800 °C with a scan rate of 10 °C/min under N_2 flux with a TG 209 F3 Tarsus instrument by (Netzsch). The complete crosslinking of the polymer matrix was assessed by attenuated total reflection Fourier-transform infrared spectroscopy (ATR-FTIR) experiments with a NicoletTM iS50 FTIR spectrometer (Thermo Scientific TM). IR spectra were collected at room temperature over the range of 4000 – 525 cm^{-1} with a resolution of 4 cm^{-1}.

The flammability test was performed by evaluating the IG behaviour when exposed to a flame in the open air. The flame was moved on the IGs and the different responses were video recorded. The

results were compared with a conventional glass fiber separator (Whatman ®) soaked with ethylene carbonate (EC): diethylene carbonate (DEC) 1:1.

Electrochemical impedance spectroscopy (EIS) measurements were performed on IGs between 100 kHz and 1 Hz at open-circuit potential using VSP-3e potentiostat (Biologic) to measure the ionic conductivity. The symmetric cells, composed of IG sandwiched between two stainless steel blocking electrodes, were assembled with ECC-Std test cells (EL-CELL GmbH). Measurements were carried out between 20 and 60 °C with a 10 °C sampling interval in a dynamic climate chamber (MKF 56, Binder). The ionic conductivity (σ) was measured following **Equation 1**:

$$\sigma = \left(\frac{l}{A}\right) \cdot \left(\frac{1}{R_s}\right) \qquad (1)$$

where l is the membrane thickness, A is the membrane surface area and R_s is the resistance value at the high-frequency intercept. The ionic conductivities were plotted versus 1000/T (K) and fitted with Arrhenius' relationship shown in **Equation 2**:

$$\sigma = \sigma_0 \cdot e^{-\frac{E_a}{kT}} \qquad (2)$$

where E_a is the activation energy, k is the Boltzmann's constant, T is the test temperature and σ_0 is the pre-exponential factor.

The electrochemical stability window (ESW) was measured with a linear sweep voltammetry test in the potential range of 2-6 V with a scan rate of 0.1 mV s^{-1}. The IGs sandwiched between a lithium foil and a stainless-steel blocking electrode were tested in ECC-Std test cells with VSP-3e potentiostat (Biologic).

The transference number was measured by Bruce, Vincent and Evans method [41,42]. A CR2032 coin cell was assembled with two lithium foil sandwiching the tested electrolyte. An EIS between 100 kHz and 0.1 Hz was carried out before and after applying a constant polarization potential of 10 mV, measuring the initial (I_o) and the steady-state (I_s) current, the initial (R_0) and the steady-state (R_s)

interfacial impedance. The lithium transference number (t_{Li^+}) was calculated according to **Equation 3**:

$$t_{Li^+} = \frac{I_S(\Delta V - I_0 R_0)}{I_0(\Delta V - I_S R_S)} \qquad (3)$$

Cyclic voltammetry (CV) tests were carried out on IGs assembled in half-cell configuration in ECC-Std test cells with VSP-3e potentiostat (Biologic) between 2.5-4.2 V at a scan rate of 0.1 mV s^{-1}. An EIS measurement was performed between 100 kHz and 0.1 Hz at open-circuit potential after every CV cycle to evaluate the internal resistance evolution of the electrolyte.

Cycling performances were investigated by assembling IGs with a LFP cathode and lithium metal anode in ECC-Std test cells. Galvanostatic charge/discharge tests were carried out at different currents ranging from 0.1 C to 1 C, at ambient temperature with an Arbin BT-2000 battery tester. As a reference, a coin cell (CR2032) referred to as Whatman PYR14 and assembled with a glass fiber separator (Whatman) soaked with LITFSI and PYR14TFSI, in the same weight ratio as mentioned in IGs production, was used to compare the electrochemical performances with 80/20 PYR14 and 80/20 PYR14 5% Al_2O_3.

Results and discussion:

The effect of Al_2O_3 NP_s on a solvent-free IG electrolyte was investigated and two different membranes were tested: 80/20 PYR14 and 80/20 PYR14 5% Al_2O_3. Both formulations were produced in a one-step preparation with thermo-initiated radical polymerization. After the curing stage, IGs were self-standing and mechanically robust allowing the separation from the glass slide, as shown in Figure 1.

The morphology of the obtained membranes was investigated by FE-SEM microscopy. As can be seen in Fig S1, Al_2O_3 NPs are evenly dispersed in the polymer matrix (Figure S1), even if some microclusters are still present. This behaviour can be ascribed to the high surface area of NPs, largely prone to aggregate. Some differences can be seen on the two membrane surfaces, the lower face in contact with the glass slide is smooth while the upper one is more inhomogeneous, with the presence

of some irregularity. This morphology is probably caused by the preparation setup with the surface not facing the glass slide resulting more irregular. As can be seen on the cross-section FE-SEM micrographs, the thickness of IGs is around 170 µm for 80/20 PYR14 5% Al_2O_3 (Figure S1.A) and 340 µm for 80/20 PYR14 (Figure S1.E). Such difference can be explained by the necessity to obtain a self-standing membrane, without additive a thickness superior to 300 µm is necessary to peel off the obtained sample from the glass slide, on the contrary with the additive an approximately 150 µm thick sample can already be peeled off, confirming the positive effect of the additive on the membranes mechanical properties. Al_2O_3 NPs have a nanometric size with a diameter of ~ 150 nm and globular shape (Figure S2).

To confirm the successful polymerization, and assess the conversion of the acrylate group, FTIR spectra were collected from the mixture of IL and a lithium salt, named IL electrolyte, from the monomer mixture before the polymerization, and the IGs after the curing step, without and with the Al_2O_3 filler. The C=C stretching vibration FTIR absorption band of the acrylate group is located at 1638 cm^{-1} and followed to assess the complete polymerization of monomers [43]. Figure 2 shows the C=C peak reduction indicating an effective curing procedure. Indeed, in both cases, the crosslinked IGs have a C=C absorption peak nearly absent compared to the monomer mixture, thus confirming the complete conversion of the double bond.

The successful crosslinking of IGs was also observed through TGA analysis showing a good thermal resistance and a single degradation step (Figure 3.A). Both formulations are stable up to 300 °C and follow a one-step degradation pathway with a maximum rate at 445 °C. 80/20 PYR14 is completely decomposed at 800°C, while for 80/20 PYR14 5 % Al_2O_3 a 1.5 % residue is still present, due to the residual Al_2O_3. Figure 3.B reports the thermograms of Al_2O_3 NPs and IL electrolyte. In the first case, a limited weight loss probably due to residual water adsorbed on the Al_2O_3 NPs is observed, while the mixture of LITFSI and PYR14TFSI presents a thermal resistance up to 380 °C and a subsequent one-step degradation path with a 7.75% residue at 800°C.

Electrolytes are one of the responsible for the thermal runaway in batteries, due to the presence of carbonate based solvents, which are very flammable [44]. Carbonates are the most used solvents for liquid electrolytes in commercial lithium batteries, possessing better performance and high Li^+ diffusivity [45,46]. For this reasons, IGs were tested under flame in the open air to evaluate their flame resistance and the results compared with a mixture of EC:DEC 1:1 (see supporting video). 80/20 PYR14 5 % Al_2O_3 shows the best performance, no smoke is released, no flames appear and the shrinkage is limited. 80/20 PYR14 is also flame resistant, but the absence of filler increases the shrinkage under heat and smoke is released. The glass fiber soaked with EC:DEC 1:1 immediately catches fire when exposed to a flame and continues until the solvents are completely consumed, with a combustion time of 13 s. The glass fiber separator was also soaked with IL electrolyte, showing no flame formation and highlighting the flame resistance properties of ILs. In Figure 4 are shown some pictures extracted from the video collected in the supporting information. This test confirms the increased safety of IGs compared to the conventional organic electrolyte in terms of limited vapour pressure and flame resistance.

To assess the applicability of the obtained IGs as electrolytes, their ionic conductivity was measured through EIS, at intervals of 10 °C, in the range of 20-60 °C. The obtained data, reported in Figure 5.A, are well fitted by the Arrhenius equation and the calculated activation energy (E_a) are 37.2 kJ mol^{-1} and 36.8 KJ mol^{-1}, respectively for electrolyte 80/20 PYR14 and 80/20 PYR14 5 % Al_2O_3, showing no particular effect of the additive on this parameter. On the contrary, the addition of Al_2O_3 NPs increases the ionic conductivity comparing to the pristine membrane. This can be explained by the surface acidic sites on Al_2O_3 NPs, attracting anions and promoting the release of free lithium ions [47]. 80/20 PYR14 5 % Al_2O_3 reaches an ionic conductivity at 20 °C of $2.05 \cdot 10^{-4}$ S cm^{-1}, considered a mandatory requirement for a good polymer electrolyte [48], and overcome 10^{-3} S cm^{-1} at 60 °C. The performances of 80/20 PYR14 are slightly lower and do not reach 10^{-3} S cm^{-1} in the temperature range investigated.

A wide ESW is essential for the electrolytes to avoid side reactions and to permit the use of new-generation electrodes like high-voltage cathodes. ILs are known to be particularly resistant at high potential and, used in combination with polymer electrolyte forming IG, constitute the ideal platform for safer batteries [49–51]. LSV tests, which results are reported in Figure 5.B, were carried out in the 2-6 V potential range with a 0.1 mV s^{-1} scan rate. The limit of the ESW was set at the point where the residual current is greater than 5 nA. Despite both IGs exhibit a large ESW due to the presence of PYR14TFSI, the addition of 5 %wt of Al_2O_3 NPs further increases the electrochemical stability from 4.8 V to 5.1 V. This improvement effect is strongly related to the interaction between the acidic surface groups of the inorganic filler and the anions, reducing its decomposition [52]. Although the interaction with anions can improve the ESW, an effect of the interactions between the polymer chains and the Al_2O_3 NPs improving anti-oxidative stability cannot be neglected [53].

Transference number was determined with Bruce, Vincent and Evans method (Eq. 3) for 80/20 PYR14 and 80/20 PYR14 5% Al_2O_3. The transference number of IGs are normally much lower than conventional liquid electrolyte, because lithium salts are not completely dissociated, forming ionic clusters [54,55]. The effective charge of these clusters can be negative (e.g. -1, -2) with a detrimental effect on the transference number due to Li^+ ions drifting in the wrong direction [56]. Nevertheless, adding Al_2O_3 NPs into the IG increases the t_{Li^+} up to 0.17 compared to 0.10 reached by no filler IG (Figure 5.C). Such an improvement is in accordance with the beneficial effect of Al_2O_3 NPs observed on the ionic conductivity.

The compatibility of the IGs with the electrodes during cycling was evaluated through cyclic voltammetry, which was performed between 2.5-4.2 V at a scan rate of 0.1 mV s^{-1}. The results show good compatibility between the IGs and the electrodes, as demonstrated in Figure 6, and a fair reversibility within different cycles, for both formulations. The 80/20 PYR14 5 % Al_2O_3 sample exhibits narrower and higher lithiation/delithiation peaks compared to no filler electrolyte, indicating a lower polarization. This can be explained by the higher transference number of this formulation,

leading to a better Li^+ transport kinetic and therefore reducing the concentration polarization of the electrolyte. In the case of 80/20 PYR14, the greater polarization could be caused both by the higher concentration gradient, due to a lower transference number, and by the formation of a thicker passivating layer which leads to a higher interfacial resistance and bigger polarization [57]. This hypothesis was confirmed by EIS measurements performed after every cycle and showed in Figure 6. EIS spectra were fitted with Z-view software and the obtained values were summarized in the supporting information (Table S1 and Table S2). For no filler electrolyte the interfacial resistance (R_2) increases in the first two cycles and then remains nearly constant, while in the case of 80/20 PYR14 5 % Al_2O_3 electrolyte, after the first cycle, the interfacial resistance (R_2) decreases, indicating a beneficial effect of Al_2O_3 NPs for the formation of a stable interfacial layer with the electrodes. The same trend can be observed in the voltage profiles of cycling performances at C/10 for a Li/LFP cell (Figure 7). The overpotential measured at 50% of the state of charge for the cell assembled with 80/20 PYR14 is significantly higher than for 80/20 PYR14 5% Al_2O_3, changing from 220 mV to 160 mV. Whatman glass fiber separator soaked with IL electrolyte obtains the highest value of overpotential (230 mV). This phenomenon further confirms the beneficial effect of Al_2O_3 NPs, by lowering the cell polarization, forming a better interface with the electrodes, and by improving the Li^+ transport kinetics through the cell.

The cycling performances of 80/20 PYR14 and 80/20 PYR14 5 % Al_2O_3 were assessed by sandwiching the IGs between a Li metal anode and an LFP cathode. Rate performance tests were performed at room temperature, at different current densities, ranging from C/10 to 1C. Adding Al_2O_3 NPs to the formulation increases the electrochemical performance up to ~ 125 mAh g^{-1} at C/10 compared to ~ 100 mAh g^{-1} obtained in the same condition by the no-filler IG, as shown in Figure 8. The same behaviour is observed in the full range of current densities investigated where the beneficial effect of Al_2O_3 NPs can be detected. Coulombic efficiencies (CE) are close to 100 % for both formulations, 80/20 PYR14 5 % Al_2O_3 shows lower CE value after cycling at higher C-rates, reaching

then ~ 99.5 % after 100 cycles. The discharge capacity at the 25th cycle, resuming cycling at C/10, is slightly higher than the one of the 5th cycle. This can be explained by a further cell formation during the cycling at higher C-rates. On the contrary, the cell containing the no filler IG loses approximately 10% of discharge capacity when resuming the C/10 cycling (compared to the 5th cycle discharge capacity), thus demonstrating a probable loss of active material through the formation of dead lithium. For comparison a Whatman glass fiber separator was soaked in the IL electrolyte used in the preparation of IGs and cycled in the same condition. As shown in Figure 8, Whatman performances are much worse compared to 80/20 PYR14 5 % Al_2O_3 indicating an important key role of the polymer backbone and additive for the ion conduction in between the electrodes. Another reason could be ascribed to the high IL viscosity, mechanically slowing Li^+ motion, and the formation of negative charged ionic cluster [56]. At 1 C the discharge capacity is almost one-third the capacity of alumina IG (Figure 8.D). Discharge capacity in the first C/10 cycles shows an increase for 80/20 PYR14 and Whatman (Figure 8.A and 8.C), suggesting an electrolyte activation is needed for the IL. The presence of Al_2O_3 NPs is beneficial on the electrolyte, because this effect is limited in 80/20 PYR14 5% Al_2O_3 favouring higher discharge capacity from the first cycles. This data confirms that the composite ionogel can withstand high current density operation thanks to its excellent ability to limit Li dendrites growth and form a stable interface, in line with the previously detailed results. Consequently, the cell polarization can be controlled, enabling higher capacity retention at higher current density. This is further verified by the Whatman cell following cycles, after the rate performance, showing inconstant cycling caused by an unstable interfacial layer which can be damaged during the Li plating/stripping process, causing the dendrites growth and leading to cell failure [58].

IGs were also tested on a long cycling test at C/5 to evaluate their capacity retention. The tests were performed at room temperature and compared as well with the Whatman separator (Figure 9). For both cells, some activation cycles are necessary to reach their maximum discharge capacity. Such value is much higher for 80/20 PYR14 5% Al_2O_3 with 112.2 mAh g^{-1} compared to the no filler IG

with 71.4 mAh g^{-1}, following then a nearly constant capacity decay of 0.1 mAh $g^{-1}cycle^{-1}$ which led to a capacity retention of 56% after 500 cycles. 80/20 PYR14 shows a lower capacity decay of 0.03 mAh $g^{-1}cycle^{-1}$ due to lower performance in the first cycles. Lower capacity retention in the first case can be also ascribed to some impurities present on NPs surface (e.g water) shown on Al_2O_3 thermograms (Figure 3), which can lead to reactions with lithium causing the capacity fade. Whatman soaked with IL electrolyte used as a reference, took more than 100 cycles to reach the maximum capacity, displaying also in this test scarce cycling performance. The cell subsequently failed approximately after 350 cycles, probably because of a short-circuit caused by dendrites growth.

Conclusions:

Employing a one-step, thermo-reticulated, solvent free radical polymerization, different IGs were prepared and characterized. The crosslinked matrix gave mechanical resistance and self-standing capability to the different formulations, even with only 20% of polymer matrix against 80% of IL. The addition of Al_2O_3 NPs was also investigated obtaining increased electrochemical performances compared to no filler electrolyte, good ionic conductivity ($2.5 \cdot 10^{-4}$ S cm^{-1} at 20 °C) and wide ESW against lithium metal (5.1 V). The improved Li^+ transport kinetics across the electrolyte and the higher transference number enhanced the performances in half-cell configuration against lithium metal anode and LFP cathode compared to no filler IG, reaching 125 mAh g^{-1} at room temperature and good capacity retention after 500 cycles. The results showed also better performances at higher current densities where the addition of Al_2O_3 NPs improved the specific capacity reaching at 1 C three times the value obtained with an IL soaked glass fiber separator. These results confirm the beneficial effect of Al_2O_3 on IGs, enhancing Li salt dissociation thanks to their surface acidic sites, attracting anions and promoting the release of free lithium ions, hence limiting ionic concentration gradient, even at higher C rates, and allowing the formation of stabler interfaces. This represents a clear opportunity to unify the safety benefits of ILs to the good performances of GPEs at room temperature, towards performant, safer and more reliable lithium metal batteries.

Acknowledgements:

The Authors want to thank Nicolò Landra for his help in the realization of the graphical abstract and Silk Sports Car for the financial support.

Bibliography:

[1] K. Xu, A Long Journey of Lithium: From the Big Bang to Our Smartphones, Energy Environ. Mater. 2 (2019) 229–233. https://doi.org/10.1002/eem2.12057.

[2] J. Xiao, Q. Li, Y. Bi, M. Cai, B. Dunn, T. Glossmann, J. Liu, T. Osaka, R. Sugiura, B. Wu, J. Yang, J.-G. Zhang, M.S. Whittingham, Understanding and applying coulombic efficiency in lithium metal batteries, Nat Energy. 5 (2020) 561–568. https://doi.org/10.1038/s41560-020-0648-z.

[3] B. Liu, J.-G. Zhang, W. Xu, Advancing Lithium Metal Batteries, Joule. 2 (2018) 833–845. https://doi.org/10.1016/j.joule.2018.03.008.

[4] D.E. Fenton, J.M. Parker, P.V. Wright, Complexes of alkali metal ions with poly(ethylene oxide), Polymer. 14 (1973) 589. https://doi.org/10.1016/0032-3861(73)90146-8.

[5] M. Armand, M. Duclot, J. Chabagno, In proceedings of the second international meeting on solid state electrolytes, in: St Andrews, Scotland, 1978.

[6] G. Feuillade, Ph. Perche, Ion-conductive macromolecular gels and membranes for solid lithium cells, Journal of Applied Electrochemistry. 5 (1975) 63–69. https://doi.org/10.1007/BF00625960.

[7] K. Luo, D. Shao, L. Yang, L. Liu, X. Chen, C. Zou, D. Wang, Z. Luo, X. Wang, Semi-interpenetrating gel polymer electrolyte based on PVDF-HFP for lithium ion batteries, Journal of Applied Polymer Science. 138 (2021) 49993. https://doi.org/10.1002/app.49993.

[8] H. Xu, D. Li, Y. Liu, Y. Jiang, F. Li, B. Xue, Preparation of halloysite/polyvinylidene fluoride composite membrane by phase inversion method for lithium ion battery, Journal of Alloys and Compounds. 790 (2019) 305–315. https://doi.org/10.1016/j.jallcom.2019.03.075.

[9] M.-C. Long, G. Wu, X.-L. Wang, Y.-Z. Wang, Self-adaptable gel polymer electrolytes enable high-performance and all-round safety lithium ion batteries, Energy Storage Materials. 53 (2022) 62–71. https://doi.org/10.1016/j.ensm.2022.08.044.

[10] H. Xu, X. Zhang, J. Jiang, M. Li, Y. Shen, Ultrathin Li7La3Zr2O12@PAN composite polymer electrolyte with high conductivity for all-solid-state lithium-ion battery, Solid State Ionics. 347 (2020) 115227. https://doi.org/10.1016/j.ssi.2020.115227.

[11] L. Zhao, Y. Huang, B. Liu, Y. Huang, A. Song, Y. Lin, M. Wang, X. Li, H. Cao, Gel polymer electrolyte based on polymethyl methacrylate matrix composited with methacrylisobutyl-polyhedral oligomeric silsesquioxane by phase inversion method, Electrochimica Acta. 278 (2018) 1–12. https://doi.org/10.1016/j.electacta.2018.05.012.

[12] A. Hosseinioun, E. Paillard, In situ crosslinked PMMA gel electrolyte from a low viscosity precursor solution for cost-effective, long lasting and sustainable lithium-ion batteries, Journal of Membrane Science. 594 (2020) 117456. https://doi.org/10.1016/j.memsci.2019.117456.

[13] H. Yang, B. Zhang, M. Jing, X. Shen, L. Wang, H. Xu, X. Yan, X. He, In Situ Catalytic Polymerization of a Highly Homogeneous PDOL Composite Electrolyte for Long-Cycle High-Voltage Solid-State Lithium Batteries, Advanced Energy Materials. 12 (2022) 2201762. https://doi.org/10.1002/aenm.202201762.

[14] H. Yang, M. Jing, H. Li, W. Yuan, B. Deng, Q. Liu, B. Ju, X. Zhang, S. Hussain, X. Shen, X. Yan, "Environment-friendly" polymer solid electrolyte membrane via a rapid surface-initiating polymeration strategy, Chemical Engineering Journal. 421 (2021) 129710. https://doi.org/10.1016/j.cej.2021.129710.

[15] J. Zhang, J. Zhao, L. Yue, Q. Wang, J. Chai, Z. Liu, X. Zhou, H. Li, Y. Guo, G. Cui, L. Chen, Safety-Reinforced Poly(Propylene Carbonate)-Based All-Solid-State Polymer Electrolyte for Ambient-Temperature Solid Polymer Lithium Batteries, Advanced Energy Materials. 5 (2015) 1501082. https://doi.org/10.1002/aenm.201501082.

[16] P.N. Didwal, Y.N. Singhbabu, R. Verma, B.-J. Sung, G.-H. Lee, J.-S. Lee, D.R. Chang, C.-J. Park, An advanced solid polymer electrolyte composed of poly(propylene carbonate) and mesoporous silica nanoparticles for use in all-solid-state lithium-ion batteries, Energy Storage Materials. 37 (2021) 476–490. https://doi.org/10.1016/j.ensm.2021.02.034.

[17] S. Skaarup, K. West, B. Zachau-Christiansen, Mixed phase solid electrolytes, Solid State Ionics. 28–30 (1988) 975–978. https://doi.org/10.1016/0167-2738(88)90314-1.

[18] W. Wieczorek, K. Such, H. Wyciślik, J. Płocharski, Modifications of crystalline structure of peo polymer electrolytes with ceramic additives, Solid State Ionics. 36 (1989) 255–257. https://doi.org/10.1016/0167-2738(89)90185-9.

[19] X. Hu, M. Jing, H. Yang, Q. Liu, F. Chen, W. Yuan, L. Kang, D. Li, X. Shen, Enhanced ionic conductivity and lithium dendrite suppression of polymer solid electrolytes by alumina nanorods and interfacial graphite modification, Journal of Colloid and Interface Science. 590 (2021) 50–59. https://doi.org/10.1016/j.jcis.2021.01.018.

[20] J. Li, L. Zhong, J. Li, H. Wu, W. Shao, P. Wang, M. Liu, G. Zhang, M. Jing, Insights into the effects of different inorganic fillers on the electrochemical performances of polymer solid electrolytes, Colloids and Surfaces A: Physicochemical and Engineering Aspects. 671 (2023) 131704. https://doi.org/10.1016/j.colsurfa.2023.131704.

[21] J. Li, R. Hu, H. Zhou, S. Tao, Y. Wang, Nano-SiO2@PMMA-doped composite polymer PVDF-HFP/PMMA/PEO electrolyte for lithium metal batteries, J Mater Sci: Mater Electron. 31 (2020) 2708–2719. https://doi.org/10.1007/s10854-019-02811-x.

[22] X. Pan, P. Yang, Y. Guo, K. Zhao, B. Xi, F. Lin, S. Xiong, Electrochemical and Nanomechanical Properties of TiO2 Ceramic Filler Li-Ion Composite Gel Polymer Electrolytes for Li Metal Batteries, Advanced Materials Interfaces. 8 (2021) 2100669. https://doi.org/10.1002/admi.202100669.

[23] J. Amici, C.A. Calderón, D. Versaci, G. Luque, D. Barraco, E. Leiva, C. Francia, S. Bodoardo, Composite polymer electrolyte with high inorganic additive contents to enable metallic lithium anode, Electrochimica Acta. 404 (2022) 139772. https://doi.org/10.1016/j.electacta.2021.139772.

[24] Y. Wang, T. Liu, C. Liu, G. Liu, J. Yu, Q. Zou, Solid-state lithium battery with garnet Li7La3Zr2O12 nanofibers composite polymer electrolytes, Solid State Ionics. 378 (2022) 115897. https://doi.org/10.1016/j.ssi.2022.115897.

[25] L. Li, R. Li, Z. Huang, H. Yang, M. Liu, J. Xiang, S. Hussain, X. Shen, M. Jing, A Multifunctional Gradient Solid Electrolyte Remarkably Improving Interface Compatibility and Ion Transport in Solid-State Lithium Battery, ACS Appl. Mater. Interfaces. 14 (2022) 30786–30795. https://doi.org/10.1021/acsami.2c05578.

[26] A. Das, M. Goswami, K. Illath, T.G. Ajithkumar, A. Arya, M. Krishnan, Synthesis and characterization of LAGP-glass-ceramics-based composite solid polymer electrolyte for solid-state Li-ion battery application, Journal of Non-Crystalline Solids. 558 (2021) 120654. https://doi.org/10.1016/j.jnoncrysol.2021.120654.

[27] S.H. Siyal, M. Li, H. Li, J.-L. Lan, Y. Yu, X. Yang, Ultraviolet irradiated PEO/LATP composite gel polymer electrolytes for lithium-metallic batteries (LMBs), Applied Surface Science. 494 (2019) 1119–1126. https://doi.org/10.1016/j.apsusc.2019.07.179.

[28] Y. Dai, S. Greenbaum, D. Golodnitsky, G. Ardel, E. Strauss, E. Peled, Y. Rosenberg, Lithium-7 NMR studies of concentrated LiI/PEO-based solid electrolytes, Solid State Ionics. 106 (1998) 25–32. https://doi.org/10.1016/S0167-2738(97)00488-8.

[29] J. Zheng, Y.-Y. Hu, New Insights into the Compositional Dependence of Li-Ion Transport in Polymer–Ceramic Composite Electrolytes, ACS Appl. Mater. Interfaces. 10 (2018) 4113–4120. https://doi.org/10.1021/acsami.7b17301.

[30] P. Fan, H. Liu, V. Marosz, N.T. Samuels, S.L. Suib, L. Sun, L. Liao, High Performance Composite Polymer Electrolytes for Lithium-Ion Batteries, Advanced Functional Materials. 31 (2021) 2101380. https://doi.org/10.1002/adfm.202101380.

[31] W. Liu, S.W. Lee, D. Lin, F. Shi, S. Wang, A.D. Sendek, Y. Cui, Enhancing ionic conductivity in composite polymer electrolytes with well-aligned ceramic nanowires, Nat Energy. 2 (2017) 1–7. https://doi.org/10.1038/nenergy.2017.35.

[32] X. Yu, A. Manthiram, A review of composite polymer-ceramic electrolytes for lithium batteries, Energy Storage Materials. 34 (2021) 282–300. https://doi.org/10.1016/j.ensm.2020.10.006.

[33] J. Fu, Z. Li, X. Zhou, X. Guo, Ion transport in composite polymer electrolytes, Mater. Adv. 3 (2022) 3809–3819. https://doi.org/10.1039/D2MA00215A.

[34] A.K. Tripathi, Ionic liquid–based solid electrolytes (ionogels) for application in rechargeable lithium battery, Materials Today Energy. 20 (2021) 100643. https://doi.org/10.1016/j.mtener.2021.100643.

[35] G. Yang, Y. Song, Q. Wang, L. Zhang, L. Deng, Review of ionic liquids containing, polymer/inorganic hybrid electrolytes for lithium metal batteries, Materials & Design. 190 (2020) 108563. https://doi.org/10.1016/j.matdes.2020.108563.

[36] D.M. Correia, L.C. Fernandes, P.M. Martins, C. García-Astrain, C.M. Costa, J. Reguera, S. Lanceros-Méndez, Ionic Liquid–Polymer Composites: A New Platform for Multifunctional Applications, Adv. Funct. Mater. 30 (2020) 1909736. https://doi.org/10.1002/adfm.201909736.

[37] S. Wen, C. Luo, Q. Wang, Z. Wei, Y. Zeng, Y. Jiang, G. Zhang, H. Xu, J. Wang, C. Wang, J. Chang, Y. Deng, Integrated design of ultrathin crosslinked network polymer electrolytes for flexible and stable all-solid-state lithium batteries, Energy Storage Materials. 47 (2022) 453–461. https://doi.org/10.1016/j.ensm.2022.02.035.

[38] W. Wu, Z. Wei, J. Wang, J. Shang, M. Wang, S.-S. Chi, Q. Wang, L. Du, T. Zhang, Z. Zheng, Y. Deng, Enabling high-energy flexible solid-state lithium ion batteries at room temperature, Chemical Engineering Journal. 424 (2021) 130335. https://doi.org/10.1016/j.cej.2021.130335.

[39] W. Zheng, W. Bi, Y. Fang, S. Chang, W. Yuan, L. Li, Solvent-Free Procedure to Prepare Ion Liquid-Immobilized Gel Polymer Electrolytes Containing Li0.33La0.56TiO3 with High Performance for Lithium-Ion Batteries, ACS Omega. 6 (2021) 25329–25337. https://doi.org/10.1021/acsomega.1c03140.

[40] Y. Liao, C. Sun, S. Hu, W. Li, Anti-thermal shrinkage nanoparticles/polymer and ionic liquid based gel polymer electrolyte for lithium ion battery, Electrochimica Acta. 89 (2013) 461–468. https://doi.org/10.1016/j.electacta.2012.11.095.

[41] J. Evans, C.A. Vincent, P.G. Bruce, Electrochemical measurement of transference numbers in polymer electrolytes, Polymer. 28 (1987) 2324–2328. https://doi.org/10.1016/0032-3861(87)90394-6.

[42] P.G. Bruce, J. Evans, C.A. Vincent, Conductivity and transference number measurements on polymer electrolytes, Solid State Ionics. 28–30 (1988) 918–922. https://doi.org/10.1016/0167-2738(88)90304-9.

[43] G. Wang, P. He, L. Fan, Asymmetric Polymer Electrolyte Constructed by Metal–Organic Framework for Solid-State, Dendrite-Free Lithium Metal Battery, Adv. Funct. Mater. 31 (2021) 2007198. https://doi.org/10.1002/adfm.202007198.

[44] A. Mauger, C.M. Julien, Critical review on lithium-ion batteries: are they safe? Sustainable?, Ionics. 23 (2017) 1933–1947. https://doi.org/10.1007/s11581-017-2177-8.

[45] A.M. Haregewoin, E.G. Leggesse, J.-C. Jiang, F.-M. Wang, B.-J. Hwang, S.D. Lin, Comparative Study on the Solid Electrolyte Interface Formation by the Reduction of Alkyl Carbonates in Lithium ion Battery, Electrochimica Acta. 136 (2014) 274–285. https://doi.org/10.1016/j.electacta.2014.05.103.

[46] Z. Yu, W. Yu, Y. Chen, L. Mondonico, X. Xiao, Y. Zheng, F. Liu, S.T. Hung, Y. Cui, Z. Bao, Tuning Fluorination of Linear Carbonate for Lithium-Ion Batteries, J. Electrochem. Soc. 169 (2022) 040555. https://doi.org/10.1149/1945-7111/ac67f5.

[47] X. Hu, M. Jing, H. Yang, Q. Liu, F. Chen, W. Yuan, L. Kang, D. Li, X. Shen, Enhanced ionic conductivity and lithium dendrite suppression of polymer solid electrolytes by alumina nanorods and interfacial graphite modification, Journal of Colloid and Interface Science. 590 (2021) 50–59. https://doi.org/10.1016/j.jcis.2021.01.018.

[48] D. Zhou, D. Shanmukaraj, A. Tkacheva, M. Armand, G. Wang, Polymer Electrolytes for Lithium-Based Batteries: Advances and Prospects, Chem. 5 (2019) 2326–2352. https://doi.org/10.1016/j.chempr.2019.05.009.

[49] X. Tang, S. Lv, K. Jiang, G. Zhou, X. Liu, Recent development of ionic liquid-based electrolytes in lithium-ion batteries, Journal of Power Sources. 542 (2022) 231792. https://doi.org/10.1016/j.jpowsour.2022.231792.

[50] K. Liu, Z. Wang, L. Shi, S. Jungsuttiwong, S. Yuan, Ionic liquids for high performance lithium metal batteries, Journal of Energy Chemistry. 59 (2021) 320–333. https://doi.org/10.1016/j.jechem.2020.11.017.

[51] N. Chen, H. Zhang, L. Li, R. Chen, S. Guo, Ionogel Electrolytes for High-Performance Lithium Batteries: A Review, Advanced Energy Materials. 8 (2018) 1702675. https://doi.org/10.1002/aenm.201702675.

[52] C.H. Park, D.W. Kim, J. Prakash, Y.-K. Sun, Electrochemical stability and conductivity enhancement of composite polymer electrolytes, Solid State Ionics. 159 (2003) 111–119. https://doi.org/10.1016/S0167-2738(03)00025-0.

[53] S. Li, S.-Q. Zhang, L. Shen, Q. Liu, J.-B. Ma, W. Lv, Y.-B. He, Q.-H. Yang, Progress and Perspective of Ceramic/Polymer Composite Solid Electrolytes for Lithium Batteries, Advanced Science. 7 (2020) 1903088. https://doi.org/10.1002/advs.201903088.

[54] M. Kunze, S. Jeong, E. Paillard, M. Schönhoff, M. Winter, S. Passerini, New Insights to Self-Aggregation in Ionic Liquid Electrolytes for High-Energy Electrochemical Devices, Advanced Energy Materials. 1 (2011) 274–281. https://doi.org/10.1002/aenm.201000052.

[55] S. Chen, S. Zhang, X. Liu, J. Wang, J. Wang, K. Dong, J. Sun, B. Xu, Ionic liquid clusters: structure, formation mechanism, and effect on the behavior of ionic liquids, Phys. Chem. Chem. Phys. 16 (2014) 5893–5906. https://doi.org/10.1039/C3CP53116C.

[56] M. Gouverneur, F. Schmidt, M. Schönhoff, Negative effective Li transference numbers in Li salt/ionic liquid mixtures: does Li drift in the “Wrong” direction?, Phys. Chem. Chem. Phys. 20 (2018) 7470–7478. https://doi.org/10.1039/C7CP08580J.

[57] L. Li, J. Wang, P. Yang, S. Guo, H. Wang, X. Yang, X. Ma, S. Yang, B. Wu, Preparation and characterization of gel polymer electrolytes containing N-butyl-N-methylpyrrolidinium bis(trifluoromethanesulfonyl) imide ionic liquid for lithium ion batteries, Electrochimica Acta. 88 (2013) 147–156. https://doi.org/10.1016/j.electacta.2012.10.018.

[58] Y. Han, B. Liu, Z. Xiao, W. Zhang, X. Wang, G. Pan, Y. Xia, X. Xia, J. Tu, Interface issues of lithium metal anode for high-energy batteries: Challenges, strategies, and perspectives, InfoMat. 3 (2021) 155–174. https://doi.org/10.1002/inf2.12166.

Figure captions

Figure 1 Picture of A) 80/20 PYR14 and B) 80/20 PYR14 5% Al_2O_3.

Figure 2 FTIR spectra of A) IL electrolyte, monomer mixture and IGs B) Zoom of previous FTIR spectra.

Figure 3 TG analysis on A) 80/20 PYR14 and 80/20 PYR14 5% Al_2O_3 and B) IL electrolyte and Al_2O_3.

Figure 4 Flammability test of A) glass fiber separator soaked in EC:DEC 1:1, B) 80/20 PYR14, C) 80/20 PYR14 5% Al_2O_3 and D) glass fiber separator soaked with IL electrolyte.

Figure 5 A) Ionic conductivity 80/20 PYR14 and 80/20 PYR14 5% Al_2O_3, B) LSV test of electrolyte 80/20 PYR14 and 80/20 PYR14 5% Al_2O_3, Chronoamperometry of C) 80/20 PYR14 and D) 80/20 PYR14 5% Al_2O_3. The insets show the EIS spectra before and after chronoamperometry.

Figure 6 CV of A) 80/20 PYR14 and B) 80/20 PYR14 5% Al_2O_3. EIS spectra measured during CV of C) 80/20 PYR14 and D) 80/20 PYR14 5% Al_2O_3.

Figure 7 Voltage profiles of A) 80/20 PYR14, B) 80/20 PYR14 5% Al_2O_3 and C) Whatman glass fiber soaked with IL electrolyte.

Figure 8 Rate performances at room temperature of A) 80/20 PYR14, B) 80/20 PYR14 5% Al_2O_3, C) Whatman soaked with IL electrolyte and D) comparison of the discharge capacity at higher C-rates.

Figure 9 Capacity retention at room temperature of A) 80/20 PYR14, B) Whatman soaked with IL electrolyte and C) 80/20 PYR14 5% Al_2O_3.

Figures

Figure 1

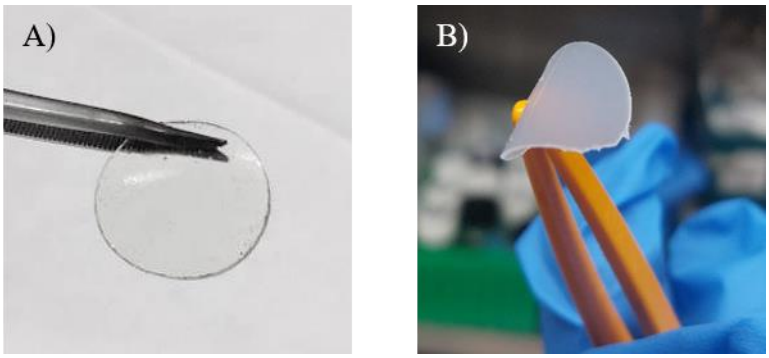

Figure 2

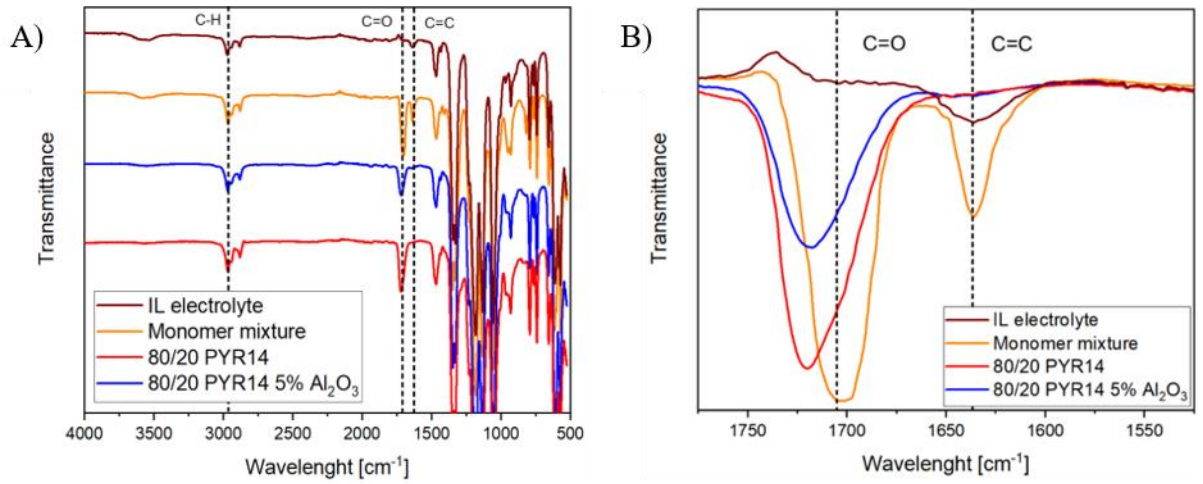

Figure 3

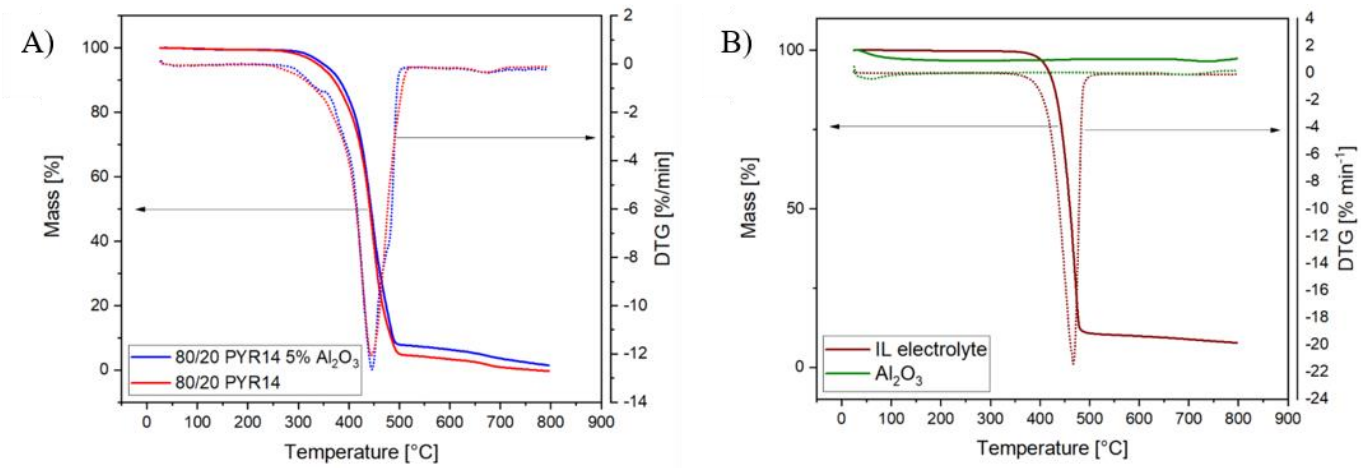

Figure 4

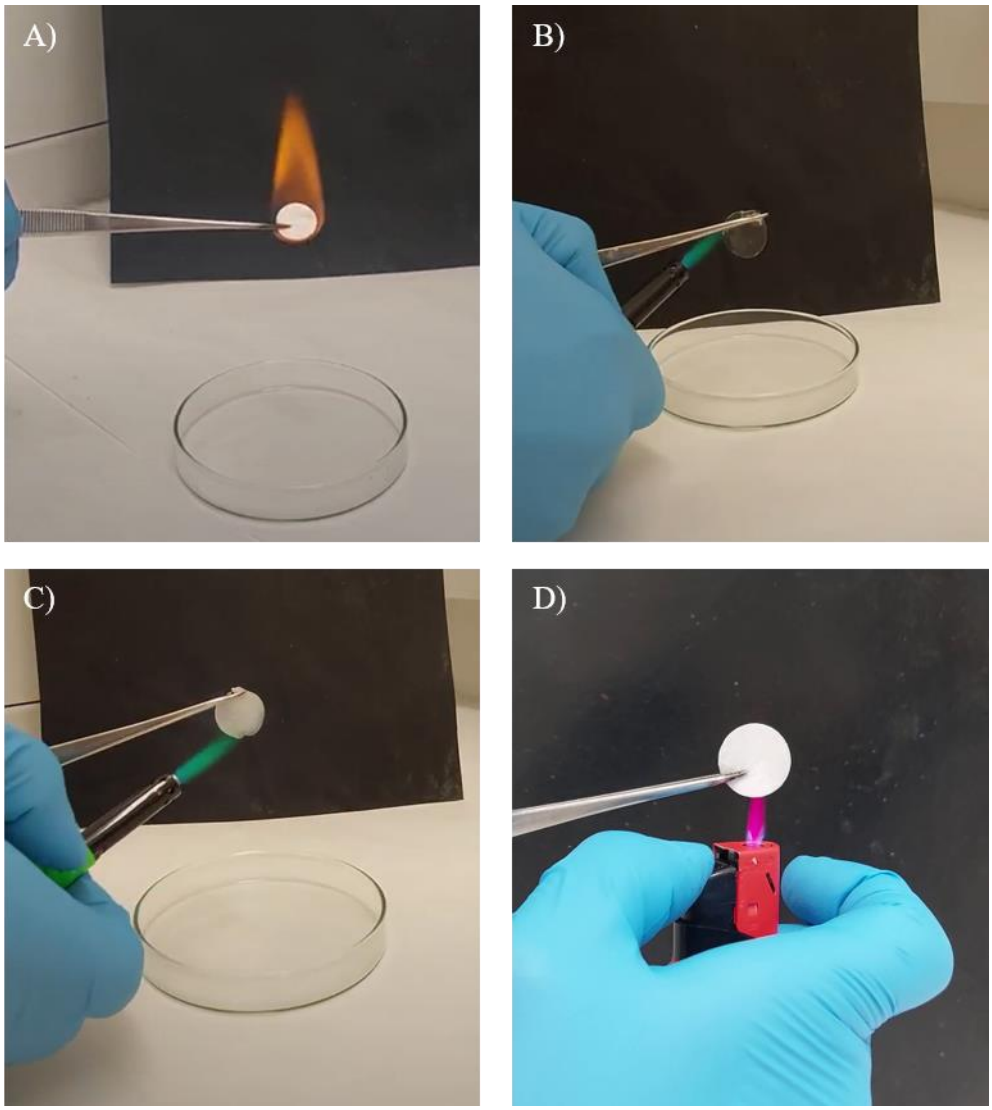

Figure 5

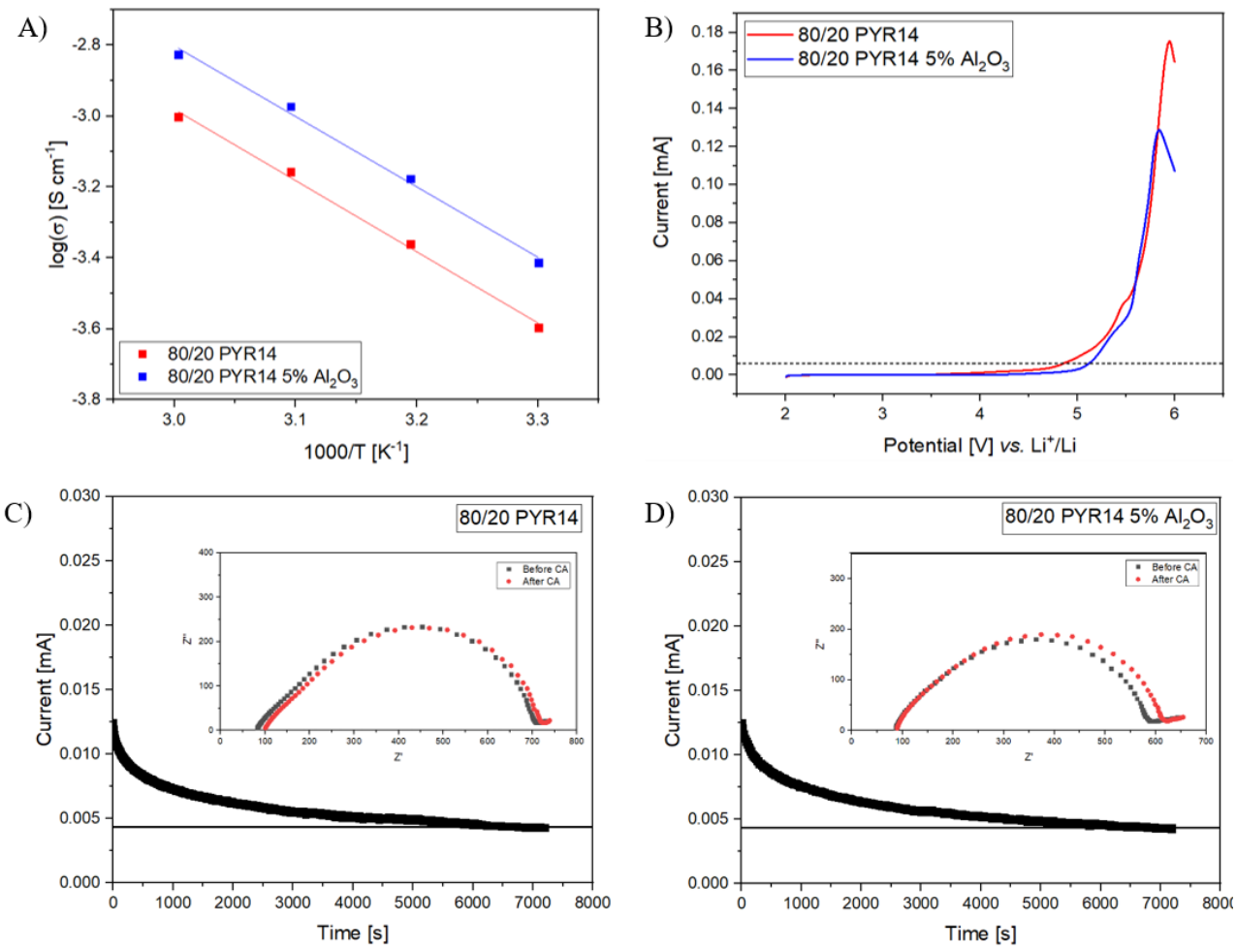
A)
log(σ) [S cm-1]
1000/T [K-1]
80/20 PYR14
80/20 PYR14 5% Al2O3
B)
Current [mA]
Potential [V] vs. Li+/Li
80/20 PYR14
80/20 PYR14 5% Al2O3
C)
80/20 PYR14
Before CA
After CA
Current [mA]
Time [s]
D)
80/20 PYR14 5% Al2O3
Before CA
After CA
Current [mA]
Time [s]

Figure 6

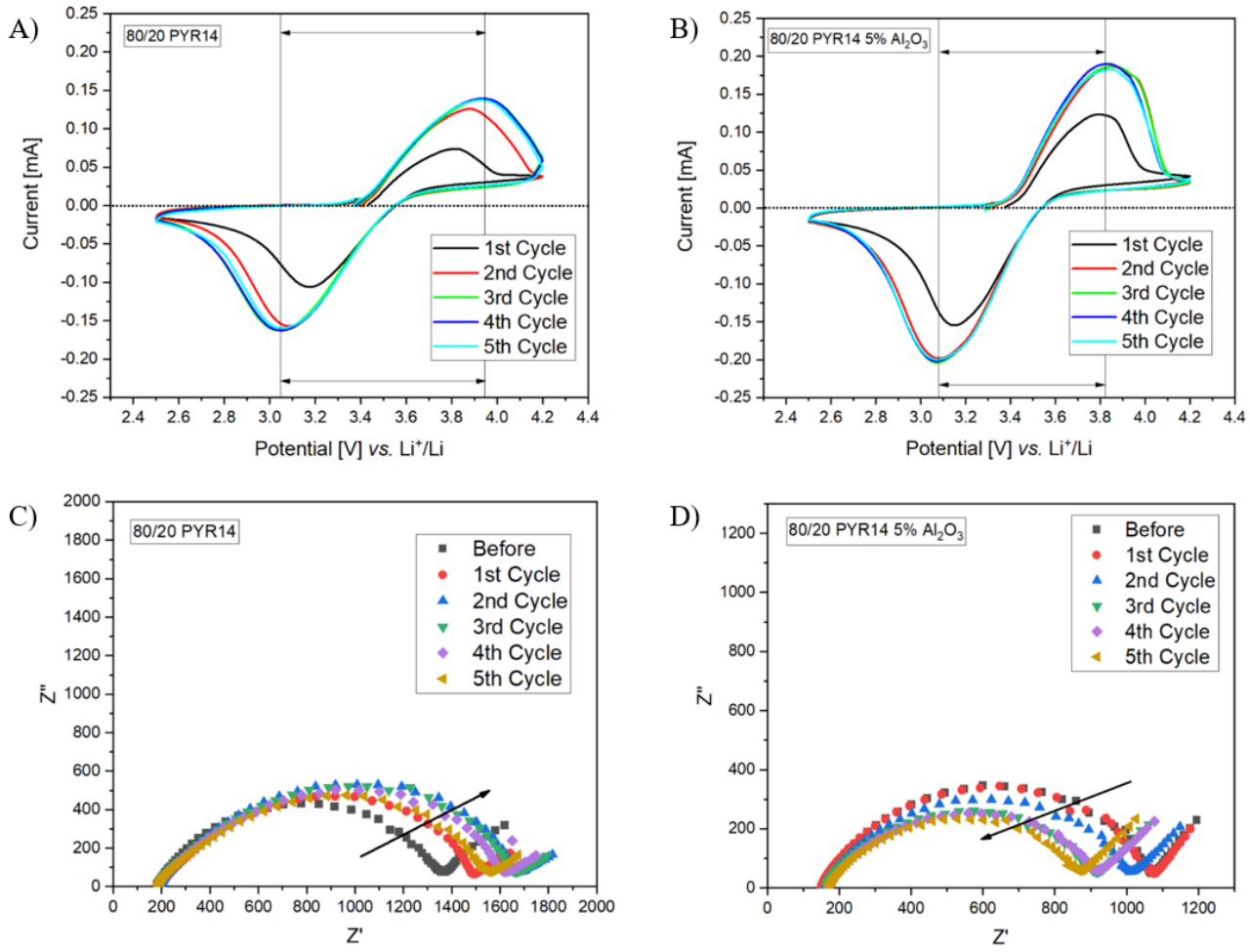
A)
80/20 PYR14
Current [mA]
Potential [V] vs. Li+/Li
1st Cycle
2nd Cycle
3rd Cycle
4th Cycle
5th Cycle
B)
80/20 PYR14 5% Al2O3
Current [mA]
Potential [V] vs. Li+/Li
1st Cycle
2nd Cycle
3rd Cycle
4th Cycle
5th Cycle
C)
80/20 PYR14
Z''
Z'
Before
1st Cycle
2nd Cycle
3rd Cycle
4th Cycle
5th Cycle
D)
80/20 PYR14 5% Al2O3
Z''
Z'
Before
1st Cycle
2nd Cycle
3rd Cycle
4th Cycle
5th Cycle

Figure 7

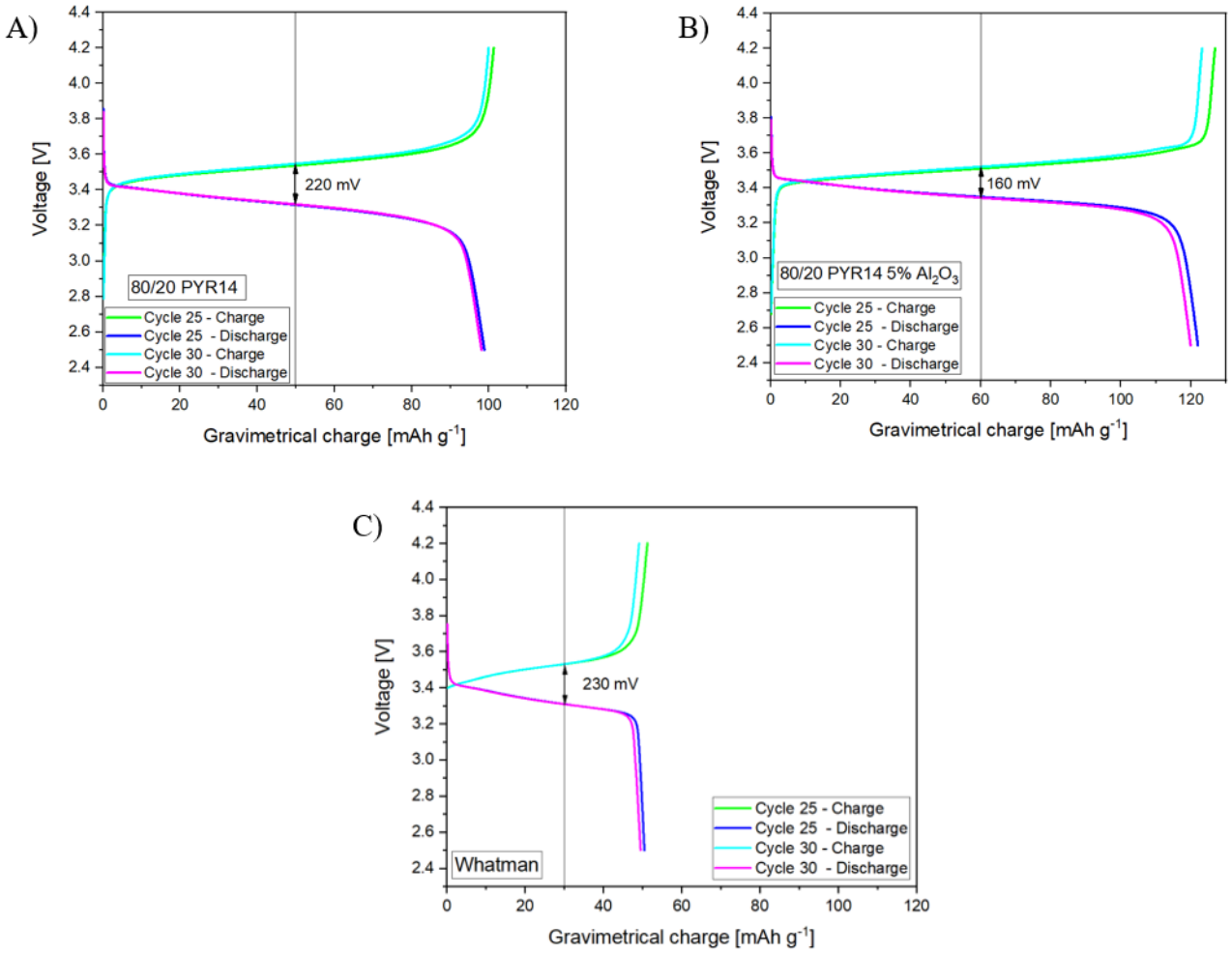
A)
Voltage [V]
Gravimetrical charge [mAh g-1]
220 mV
80/20 PYR14
Cycle 25 - Charge
Cycle 25 - Discharge
Cycle 30 - Charge
Cycle 30 - Discharge
B)
Voltage [V]
Gravimetrical charge [mAh g-1]
160 mV
80/20 PYR14 5% Al2O3
Cycle 25 - Charge
Cycle 25 - Discharge
Cycle 30 - Charge
Cycle 30 - Discharge
C)
Voltage [V]
Gravimetrical charge [mAh g-1]
230 mV
Whatman
Cycle 25 - Charge
Cycle 25 - Discharge
Cycle 30 - Charge
Cycle 30 - Discharge

Figure 8

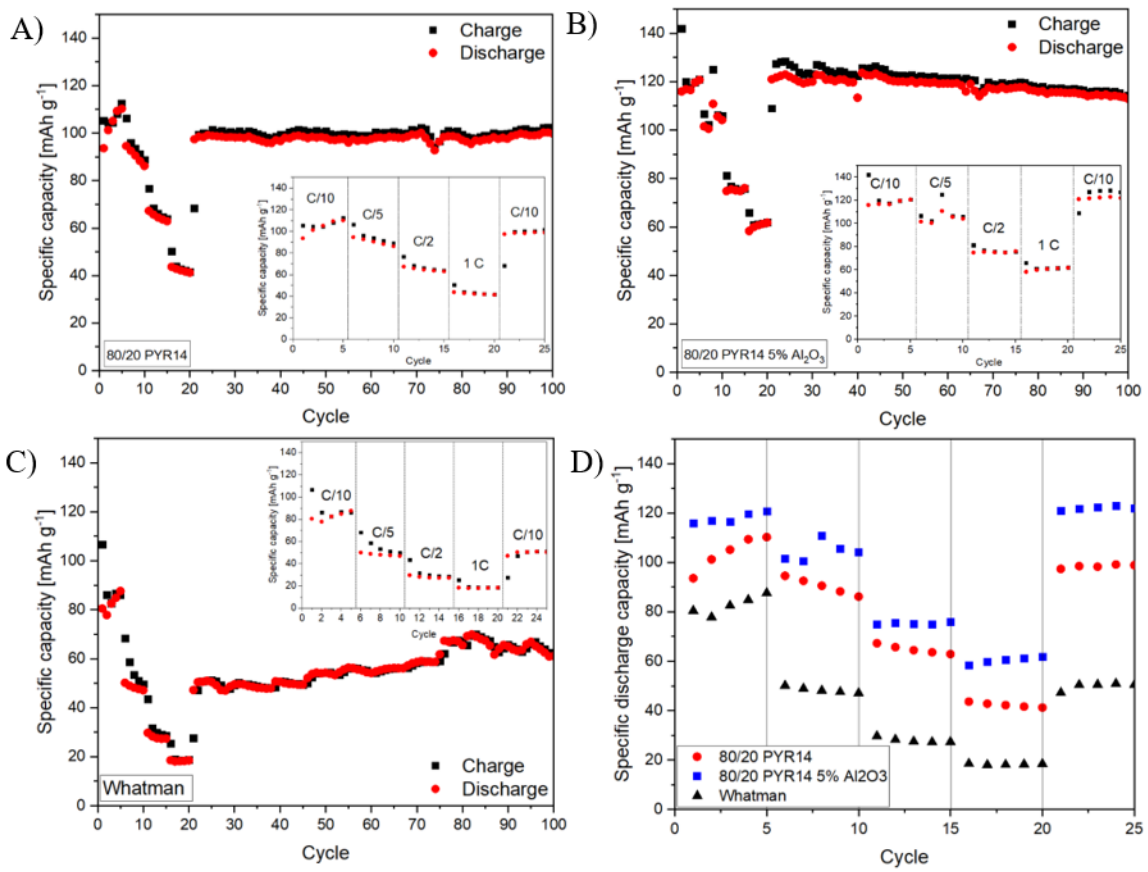
A)
Charge
Discharge
Specific capacity [mAh g-1]
Cycle
80/20 PYR14
C/10
C/5
C/2
1 C
C/10
B)
Charge
Discharge
Specific capacity [mAh g-1]
Cycle
80/20 PYR14 5% Al2O3
C/10
C/5
C/2
1 C
C/10
C)
Specific capacity [mAh g-1]
Cycle
Whatman
C/10
C/5
C/2
1C
C/10
Charge
Discharge
D)
Specific discharge capacity [mAh g-1]
Cycle
80/20 PYR14
80/20 PYR14 5% Al2O3
Whatman

Figure 9

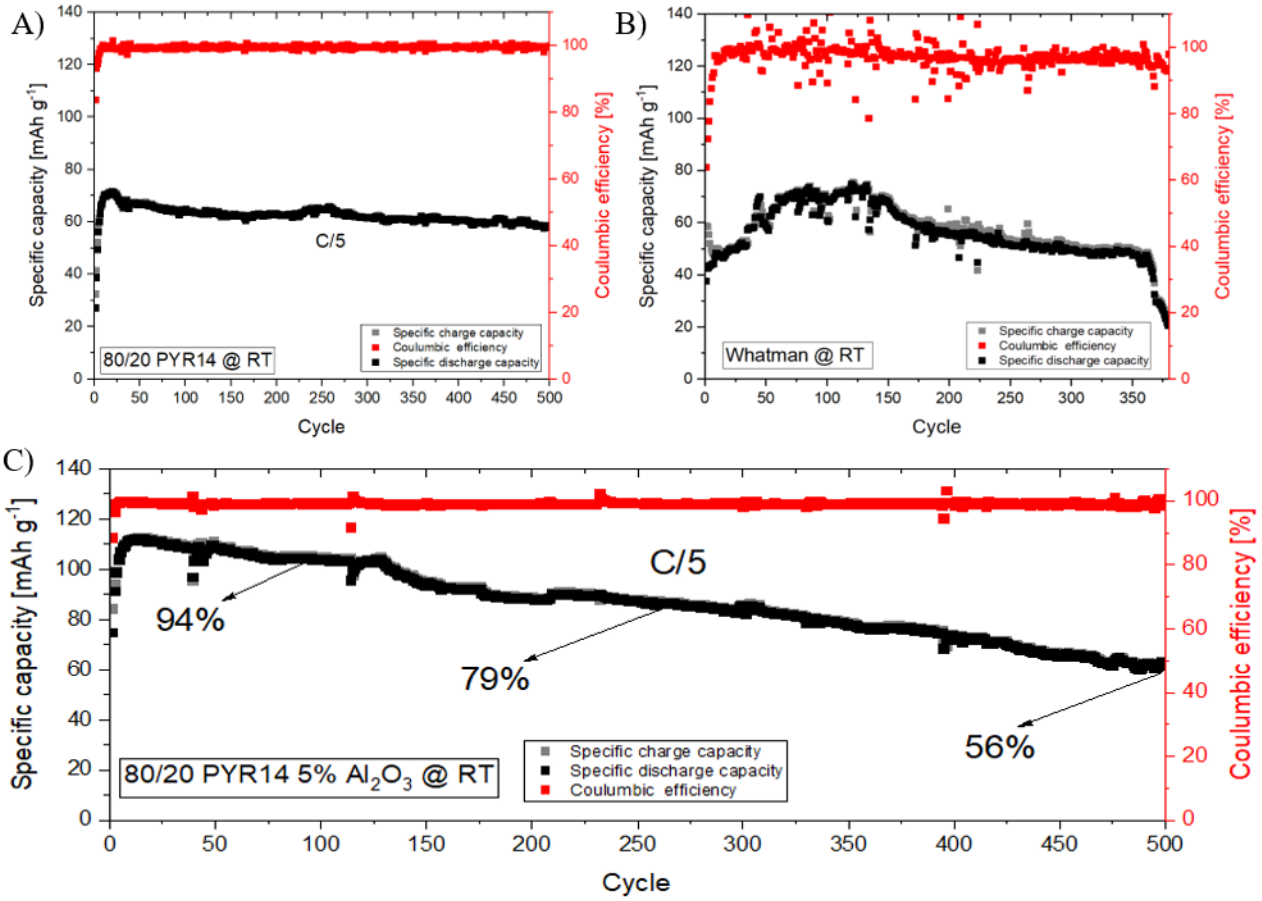
A)
Specific capacity [mAh g-1]
Coulumbic efficiency [%]
Cycle
C/5
80/20 PYR14 @ RT
Specific charge capacity
Coulumbic efficiency
Specific discharge capacity
B)
Whatman @ RT
C)
94%
79%
56%
80/20 PYR14 5% Al2O3 @ RT